

Is Hydrogen Diffusion along Grain Boundaries Fast or Slow? Atomistic Origin and Mechanistic Modeling

Xiao Zhou,¹ Normand Mousseau,² and Jun Song^{1,*}

¹*Department of Materials Engineering, McGill University, Montréal, Quebec H3A0C5, Canada*

²*Département de physique and Regroupement québécois sur les matériaux de pointe, Université de Montréal, C.P. 6128, Succursale Centre-Ville, Montréal, Québec H3C 3J7, Canada*



(Received 27 February 2019; published 29 May 2019)

We perform comprehensive first-principles calculations and kinetic Monte Carlo simulations to explicitly elucidate the distinct roles of grain boundaries (GBs) in affecting hydrogen (H) diffusion in fcc nickel (Ni). We demonstrate the transition between slow and fast H diffusion along the GB with an abrupt change in H diffusivity. Low-angle GBs are shown to comprise isolated high-barrier regions to trap and inhibit H diffusion, with H diffusivity well prescribed by the classical trapping model, while high-angle GBs are shown to provide interconnected low-barrier channels to facilitate H transport. On the basis of the dislocation description of the GB and the Frank-Bilby model, the slow-fast diffusion transition is identified to result from dislocation core overlapping and is accurately predicted. The present Letter provides key mechanistic insights towards interpreting various experimental studies of H diffusion in metals, new critical knowledge for predictive modeling of H embrittlement, and better understanding of the kinetics of H and other interstitial impurities in microstructures.

DOI: [10.1103/PhysRevLett.122.215501](https://doi.org/10.1103/PhysRevLett.122.215501)

Hydrogen embrittlement (HE), a phenomenon where hydrogen (H) causes premature failure with a drastic loss in ductility, toughness, and strength in metals, in particular, high-strength metals, has been a topic of intense research for decades [1–7]. Although the exact microscopic mechanism underlying HE remains elusive and highly debated [2,8–11], it is commonly agreed that one prerequisite for HE to occur is for H to be delivered to target regions at critical concentration. The target region is, in general, a stress-concentrated location (more often also a “defective” location, e.g., microcrack, grain boundary, nanovoid, etc.) and the critical concentration is the threshold H concentration that induces a change in the deformation mode (i.e., from the normal ductile deformation to brittlelike deformation behaviors [2,12]). Consequently, understanding this phenomenon requires an accurate knowledge of H transport in metals to provide a correct interpretation of various HE data and phenomena.

The effect of microstructures on H diffusion in metals has been well recognized and studied in the literature [3,13–16]. In particular, H segregation and diffusion along grain boundaries (GBs) are crucial for H-induced intergranular cracking [17–21]. Nonetheless, different—and even contrary—viewpoints exist regarding the exact role of GBs in H diffusion. Numerous studies have reported accelerated H transport along GBs [7,17–20,22–27], which was attributed to low activation barriers and short-circuit diffusion along GBs [19,27,28]. However, there also exists ample evidence of the opposite observation [18,29–32]. For instance, Yao and Cahoon [30] discovered that, at

extremely low H concentration, H is virtually stopped at GBs, indicating strong retardation of H motion by GBs. More recently, Oudriss *et al.* [33–35] demonstrated the strong dependence of H diffusion behaviors on GB characteristics and grain size, suggesting that H diffusion can be facilitated by random high-angle GBs while being inhibited by special GBs.

The high contention regarding the effect of GBs in H diffusion indicates a clear lack of mechanistic understanding, a knowledge deficit we aim to address in this Letter. Employing comprehensive first-principles calculations and kinetic Monte Carlo (KMC) simulations, we explicitly elucidated the dual role of GBs in H diffusion and its dependence on the GB structure and H bulk concentration, using nickel (Ni) as a model system. The atomistic origin underlying the multiplex GB effect on H diffusion was clarified and a mechanistic model was proposed to predict transitions between distinct diffusion behaviors. Our Letter sheds critical new light on understanding and interpreting the various experimental studies of H diffusion in metals, being an important step towards the formation of a unified option of GBs in H kinetics and H embrittlement in metals.

A series of symmetric tilt GBs of different tilt angles in Ni were examined in our study, with a few representative configurations presented in Fig. 1. The GB structure (and adjacent bulk lattice) was analyzed utilizing the space tessellation approach proposed in Zhou *et al.* [36], which characterizes the GB structure as an array of joint polyhedrons. The approach enables quick search and identification of H adsorption sites (as encapsulated in individual

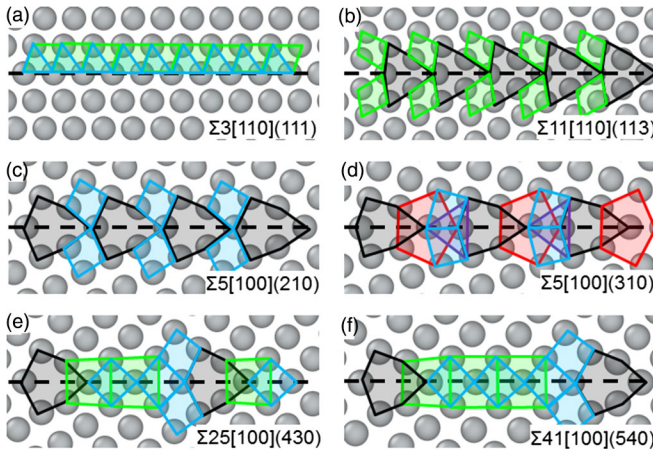


FIG. 1. Representative GB configurations examined in this Letter, (a) $\Sigma 3[110](111)$, (b) $\Sigma 11[110](113)$, (c) $\Sigma 5[100](210)$, (d) $\Sigma 5[100](310)$, (e) $\Sigma 25[100](430)$, and (f) $\Sigma 41[100](540)$, with the polyhedral units constituting the GB illustrated. The gray spheres indicate the host Ni atom. Different polyhedral units, i.e., octahedron (OCT), tetrahedron (TET), capped-trigonal prism (CTP), bitetrahedron (BTE), and pentagonal bipyramid (PBP) are indicated by different geometrical shapes in green, blue, gray, purple, and red shades, respectively.

polyhedrons) and H migration paths (with H diffusion being hops between adjacent polyhedrons), aided by which the exact locations of interstitial sites and associated energetics and energy barriers of H were then determined from density functional theory calculations (see Supplemental Material for details [37]). Figure 2 shows contour mappings of energy barriers for H diffusion at several representative GBs. To put those results into context, it is worth noting that the migration barrier of H diffusion in bulk Ni lattice was determined to be 0.38 eV [0.42 eV with zero point energy (ZPE) correction [52]], in agreement with previous theoretical (0.37 eV [53]) and experimental (0.4 eV [54]) studies. One note to make is that the influence of ZPE correction has been investigated by benchmark calculations (see Supplemental Material for details [37]), and we found that ZPE does not really affect the spatial landscape and relative values of H energetics and migration barriers, despite causing a slight shift in the absolute values. This is in accordance with the previous work performed by Stefano *et al.* [55], where it was shown that the quantum mechanical effect on H diffusion can be important for an accurate assessment of H migration in bcc Fe, but to a much less degree in fcc Ni. Therefore, below we only present results without the ZPE correction.

Figure 2 depicts typical scenarios of H migration at GBs. First, we note that there exist certain GBs where H migration has similar energy barriers as that of bulk diffusion, indicative of little alternation of H diffusion behaviors by those GBs. Figures 2(a) and 2(b) show two representative GBs of this kind, i.e., $\Sigma 3[110](111)$ and $\Sigma 11[110](113)$, both of which are confirmed by

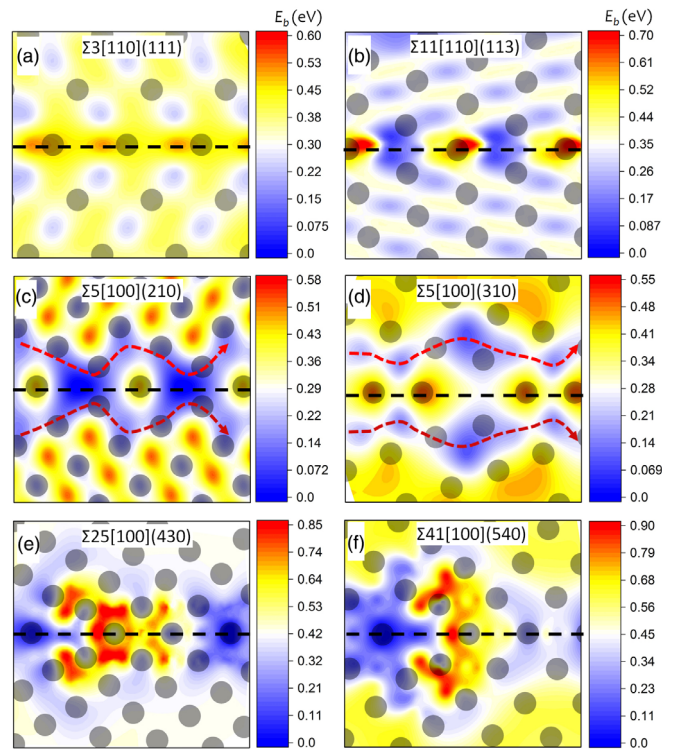


FIG. 2. Contour mapping of the energy barrier E_b of H migration at representative GBs. (a) $\Sigma 3[110](111)$, (b) $\Sigma 11[110](113)$, (c) $\Sigma 5[100](210)$, (d) $\Sigma 5[100](310)$, (e) $\Sigma 25[100](430)$, (f) $\Sigma 41[100](540)$. Big gray spheres represent host Ni atoms.

experiments [17,35,56] to exhibit *bulklike* diffusion behaviors. Meanwhile, there are apparent cases of H migration greatly modified by GBs. As shown in Figs. 2(c) and 2(d), GBs provide interconnected low-barrier paths to facilitate H transport along the GB, while in GBs shown in Figs. 2(e) and 2(f), there exist high-barrier regions that would presumably inhibit or disrupt H transport along the GB.

The results in Fig. 2 clearly demonstrate the significant influence of GBs on local H migration, similar to what was observed recently on C diffusion in Fe [57]. KMC simulations with the density functional theory-calculated energy barriers as input were then conducted to examine collective diffusion behaviors of H. Figure 3 shows H diffusivity data (along GB direction) extracted from KMC simulations for systems containing different GBs as functions of H bulk concentration C_b and temperature T . Consistent with the different scenarios of H migration at GBs (cf. Fig. 2), distinct diffusivities (and their evolution as C_b varies) are observed. Examining the diffusivity data at room temperature (i.e., 300 K), the $\Sigma 3[110](111)$ and $\Sigma 11[110](113)$ GB systems [cf. Figs. 3(c) and 3(d)] exhibit almost identical D vs C_b evolution as the bulk lattice, where D stays constant until the lattice is saturated with H, attributed to the minimal influence of GBs on the hydrogen migration barrier. For the $\Sigma 5[100](210)$ and $\Sigma 5[100](310)$ GB systems [cf. Figs. 3(e) and 3(f)], D is much higher

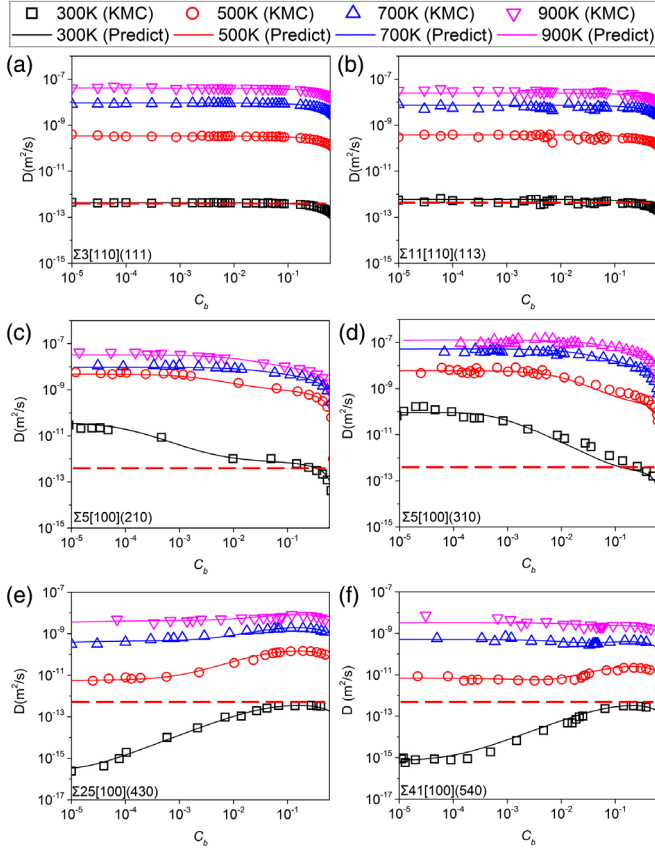


FIG. 3. H diffusivity (D) as H bulk concentration (C_b) varies, calculated from KMC simulations and predicted from Eq. (1), for GBs: (a) $\Sigma 3[110](111)$, (b) $\Sigma 11[110](113)$, (c) $\Sigma 5[100](210)$, (d) $\Sigma 5[100](310)$, (e) $\Sigma 25[100](430)$, and (f) $\Sigma 41[100](540)$, at different temperatures.

than the bulk value at low C_b , but continues to decrease as C_b increases. In contrast, the $\Sigma 25[100](430)$ and $\Sigma 41[100](540)$ GB systems show much lower D than the bulk value at low C_b , with D monotonically increasing as C_b increases. Such strong dependence of D on C_b observed in Figs. 3(c) and 3(d) or Figs. 3(e) and 3(f) is due to how GB diffusion dominates at low C_b , while at high C_b , bulk diffusion becomes significant due to GB saturation. Meanwhile, we see that the influence of GBs on H diffusivity diminishes as temperature increases, which can be attributed to thermally facilitated H exchange between the GB and bulk lattice.

The numerical results from KMC simulations may also be described by an analytical expression, with the diffusivity approximated as the weighted sum of contributions from different interstitial sites over the whole lattice [58,59],

$$D(T, C_b) = \sum_i p_i(T) D_{0,i} \exp\left(\frac{-\Delta E_i}{k_B T}\right) \times \Theta_i(T, C_b), \quad (1)$$

where $p_i(T)$ denotes the probability of finding H at interstitial site i , $\Theta_i(T, C_b)$ is the blocking coefficient at

site i , and $D_{0,i}$ and ΔE_i , respectively, denote the associated diffusion prefactor and dominant energy barrier (see Supplemental Material for details [37]). As illustrated in Fig. 3, the predicted diffusivities from Eq. (1) are in good agreement with those from KMC simulations. This confirms the accuracy of Eq. (1) in describing H diffusion behaviors at GBs and shows that the modification of diffusivity comes from the combined GB effects on site occupancy and the migration barrier of H.

One approximation made in the KMC simulations is that we did not consider the influence of a H–H interaction. In a previous study by Mütschle and Kirchheim [60] on H segregation and diffusion at GBs in nanocrystalline Pd, it was demonstrated that H–H interaction plays a minor role in bulk H concentration up to 0.01 H/Pd. Given that the H–H interaction energy in Ni (~ -0.04 eV) is much weaker than that (~ -0.31 eV) in Pd and in the absence of large stress concentration, we therefore expect the H–H interaction to have a negligible effect on H segregation and diffusion in Ni for the range of H concentration (i.e., $C_b < 0.01$, see Fig. 4) in which we are interested, which is also further confirmed by a few benchmark calculations we performed.

Further examination of H diffusion behaviors revealed that H diffusivity exhibits critical dependence on the GB tilt angle θ . For a systematic discussion, here we choose symmetric tilt GBs with $[100]$ tilt axis as the representative group, where the tilt angle θ ranges between 0° and 90° . As seen in Fig. 4(a), slow diffusion is observed for θ smaller than 28° or larger than 62° , while fast diffusion is observed for θ ranging between 28° and 62° . Interestingly, we note that fast diffusion occurs exclusively along high-angle GBs, while for slow-diffusion regimes, the diffusivity (for a particular C_b) decreases monotonically as θ increases

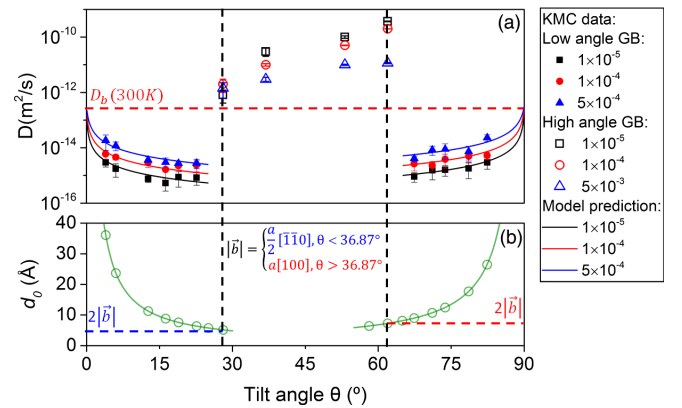


FIG. 4. (a) H diffusivities at different H bulk concentration C_b as functions of the GB tilt angle θ at 300 K. The horizontal red dashed line indicates bulk H diffusivity at 300 K and the solid lines are predictions from Eq. (3). (b) Dislocation separation distance along the GB as a function of θ according to the Frank-Bilby model (2), where \vec{b} denotes the Burgers vector of the constituting dislocation.

(or decreases from 90° for $\theta > 62^\circ$). (Note that the regime of tilt angle $> 62^\circ$ is effectively the low-angle regime considering the crystal symmetry.)

To understand such variation in H diffusivity, we note that a low-angle tilt GB can be described as a planar array of dislocations. Based on the Frank-Bilby model [61–63], there exist two Frank-Bilby Burgers vectors for dislocations constituting [100] tilt GBs, i.e., with $\vec{b} = a/2[\bar{1}\bar{1}0]$ for $\theta < 36.87^\circ$ and $\vec{b} = a[100]$ for $\theta > 36.87^\circ$, with the spacing d_0 between adjacent dislocations being

$$d_0 = \frac{|\vec{b}|}{2 \sin(\varphi/2)}, \quad \text{with} \quad \begin{cases} \vec{b} = a/2[\bar{1}\bar{1}0] & \text{and } \varphi = \theta & \text{for } \theta < 36.87^\circ \\ \vec{b} = a[100] & \text{and } \varphi = 90^\circ - \theta & \text{for } \theta > 36.87^\circ \end{cases} \quad (2)$$

As φ increases, spacing between dislocations along the GB decreases, as illustrated in Fig. 4(b). For small φ , the dislocations act as individual trapping sites and create localized high-barrier regions along GBs, as previously demonstrated in Figs. 2(e) and 2(f). Consequently, slow diffusion is expected. Combining the Frank-Bilby model with the McNabb-Foster trapping formulation [13,64] (see Supplemental Material for details [37]), H diffusivity can be predicted as

$$D = \frac{D_b}{1 + \frac{C_T}{C_b} \left(1 - \frac{C_T \times d_{GB}}{2\pi|\vec{b}|N_b \sin(\varphi/2)} \right)}, \quad (3)$$

where C_T is the H concentration at the trapping site (i.e., dislocation), D_b is the H diffusivity in bulk lattice, N_b is the number of bulk lattice sites per volume, and d_{GB} is the grain size, while \vec{b} and φ were previously defined in Eq. (2). As seen in Fig. 4(a), Eq. (3) well predicts the tilt angle and concentration dependence of H diffusivity for low-angle GBs. This also confirms that the downward trend in H diffusivity (as φ increases) for GBs in slow-diffusion regimes originates from the increase of trapping (dislocation) density along the GB.

As φ continues to increase, the spacing between dislocations further decreases. Eventually, dislocation cores start to overlap and it is no longer possible to distinguish individual dislocations along the GB. The transition from individual dislocations to core overlapping can be precisely identified by examining the evolution of the polyhedrons that constitute the GB as the tilt angle varies (see Supplemental Material for details [37]). This is found to nicely coincide with the dislocation spacing being 2 times the Burgers vector, i.e., $d_0 = 2|\vec{b}|$, namely, taking the effective core radius as $|\vec{b}|$. Plugging this condition into the Frank-Bilby equation (2), we can then precisely

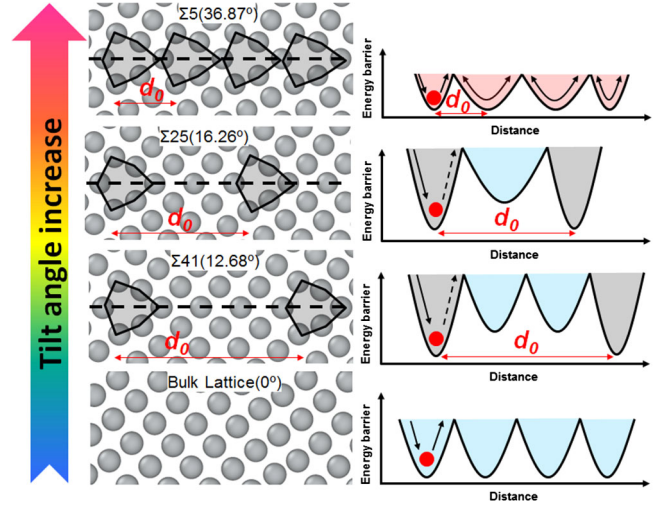


FIG. 5. Schematic illustration of dislocation cores at GBs and the evolution of energy barrier with tilt angle increase. The gray shape represents dislocation cores at GBs. The gray spheres are the host Ni atom and the small red ball illustrates the H atom.

determine the range of tilt angle in which dislocation core overlapping occurs to be 28.95° and 61.05° , which interestingly coincides with the range of tilt angle when fast diffusion occurs, as depicted in Fig. 4(a). Such nice correspondence is identified to be attributed to the fact that the core overlapping induces substantial volume dilation to key GB polyhedrons responsible for the rate-limiting diffusion steps (see Supplemental Material for details [37]), thereby effectively rendering the formation of interconnected low-barrier paths for H diffusion [e.g., see Figs. 2(c) and 2(d)], as schematically illustrated in Fig. 5. Consequently, the core overlapping directly corresponds to the abrupt elevation of H diffusivity in the regime of high-tilt angles.

Figure 4 also shows that increasing C_b , respectively, increases and decreases H diffusivity in slow- and fast-diffusion regimes, towards the bulk H diffusivity D_b . This can be well attributed to GBs being the thermodynamically preferential location for H adsorption. Increasing H bulk concentration thus leads to saturation of GB sites and, subsequently, the overall H diffusivity is more contributed by bulk H diffusion.

To conclude, we have explicitly demonstrated the distinct roles GBs may assume in affecting H diffusion and elucidated their dependence on the GB structure, through comprehensive first-principles calculations and KMC simulations. Using symmetric tilt GBs with a [100] tilt axis as the representative, we quantitatively showcased the transition between slow H diffusion and fast H diffusion along the GB with an abrupt change in H diffusivity, as the GB tilt angle varies. We showed that low-angle GBs comprise isolated high-barrier regions that trap and inhibit H diffusion, while high-angle GBs provide interconnected low-barrier channels that facilitate H transport. Using the

dislocation description of GB of the Frank-Bilby model, we identified the slow-fast diffusion transition that results from dislocation core overlapping; we also accurately predicted the threshold angle at which such transition occurs. Finally, we showed that the H diffusivity for low-angle GBs can be well described by the classical trapping model treating constituting dislocations as discrete trap sites.

The present Letter provides important mechanistic insights to interpret and understand the often bipolar experimental observation of the GB effect on H diffusion in Ni, in accordance with numerous experimental evidence showing low-angle GBs causing slow diffusion [31,33,34], and high-angle and/or random GBs accelerating H diffusion [33–35]. Our findings are also generally applicable to H diffusion in other structural metals, as well evidenced by the recent work of Iwaoka *et al.* [65] on H diffusion in fcc Pd, which demonstrated the random high-angle boundaries as fast-diffusion paths and the strong impediment of H diffusion by dislocations, and the silver-decoration experiment by Koyama *et al.* [66], showing that H flux through low-angle GBs in steel is drastically lower than that through high-angle GBs. Moreover, our Letter has clarified the notable dependence of H diffusivity on H bulk concentration, showing that the increasing H lattice population would moderate the effect of GBs on H diffusion. This reflects the important influence of the chemical environment (e.g., chemical potential, charging current, etc.), suggesting that caution should be used in interpreting H diffusion experiments.

Meanwhile, worthy of note is the two-dimensional nature of GBs, and therefore, in addition to the along-GB diffusion, there is also the contribution of H diffusion along the tilt axis direction. With the lattice structure along the tilt axis following a different pattern, such contribution would presumably exhibit different dependence on the GB angle (or other GB metrics). Consequently, further research efforts are needed in future studies to obtain a more complete picture of the GB-mediated H diffusion.

Furthermore, our findings on H diffusion may also provide useful hints for understanding the diffusion behaviors of other impurities in metals. For instance, Leonhardt *et al.* [67] experimentally investigated oxygen diffusion in SrTiO₃ bicrystals and also found that the Σ 3 twin boundary has no effect on diffusion, while low-angle Σ 13 GB exhibits a pronounced resistance. Couling and Smoluchowski [68] conducted a comprehensive investigation of Ag diffusion behaviors along [100] tilt GBs in Cu and revealed a strong correlation between impurity penetration and the GB angle (see Supplemental Material for details [37]) that shows a strikingly resemblance to what we demonstrated in Fig. 4. Such observed similarity in the dependence of diffusion on GB characteristics for different impurities, despite variance in the detailed diffusion process and/or the diffusion mechanism, further alludes to the possibility of a more generic structure-property relationship

underlying the GB-mediated diffusion of impurities, a topic probably worthy of further investigation.

The authors are grateful to Professor William A. Curtin for fruitful discussions and valuable suggestions. X. Z. and J. S. acknowledge the support of the Natural Sciences and Engineering Research Council of Canada (NSERC Discovery Grant No. RGPIN 418469-2012) and China Scholarship Council (CSC). The authors also acknowledge the computational support provided by Consortium Laval UQAM McGill and Eastern Quebec (CLUMEQ).

*Corresponding author.

jun.song2@mcgill.ca

- [1] W. H. Johnson, *Proc. R. Soc. London* **23**, 168 (1874).
- [2] A. R. Troiano, *Trans. Am. Soc. Met.* **52**, 54 (1960).
- [3] P. Cotterill, *Prog. Mater. Sci.* **9**, 205 (1961).
- [4] M. Louthan, G. Caskey, J. Donovan, and D. Rawl, *Mater. Sci. Eng.* **10**, 357 (1972).
- [5] R. Oriani, *Ber. Bunsen-Ges. Phys. Chem.* **76**, 848 (1972).
- [6] H. Johnson, *Science* **179**, 228 (1973).
- [7] A. M. Brass, A. Chanfreau, and J. Chêne, Role of grain boundaries and cold work on hydrogen permeation in nickel, in *Hydrogen Effects on Material Behaviour*, edited by N. R. Moody and A. W. Thompson (, Trans. Metall. Soc., Warrendale, PA, 1990), pp. 19–31.
- [8] I. Robertson and H. Birnbaum, *Acta Metall.* **34**, 353 (1986).
- [9] H. K. Birnbaum and P. Sofronis, *Mater. Sci. Eng. A* **176**, 191 (1994).
- [10] T. Neeraj, R. Srinivasan, and J. Li, *Acta Mater.* **60**, 5160 (2012).
- [11] J. Song and W. Curtin, *Nat. Mater.* **12**, 145 (2013).
- [12] R. Oriani and P. Josephic, *Acta Metall.* **22**, 1065 (1974).
- [13] R. A. Oriani, *Acta Metall.* **18**, 147 (1970).
- [14] V. M. Sidorenko and I. I. Sidorak, *Mater. Sci.* **9**, 372 (1975).
- [15] J. Völkl and G. Alefeld, in *Hydrogen in Metals I: Basic Properties*, edited by G. Alefeld and J. Völkl (Springer, Berlin, 1978), p. 321.
- [16] R. Kirchheim, F. Sommer, and G. Schluckebier, *Acta Metall.* **30**, 1059 (1982).
- [17] B. Ladna and H. K. Birnbaum, *Acta Metall.* **35**, 2537 (1987).
- [18] A. Kimura and H. K. Birnbaum, *Acta Metall.* **36**, 757 (1988).
- [19] T. M. Harris and M. Latanision, *Metall. Trans. A* **22**, 351 (1991).
- [20] G. Palumbo, D. M. Doyle, A. M. El-Sherik, U. Erb, and K. T. Aust, *Scr. Metall. Mater.* **25**, 679 (1991).
- [21] P. Hicks and C. Altstetter, *Metall. Trans. A* **23**, 237 (1992).
- [22] R. D. Calder, T. S. Elleman, and K. Verghese, *J. Nucl. Mater.* **46**, 46 (1973).
- [23] T. Tsuru and R. M. Latanision, *Scr. Metall.* **16**, 575 (1982).
- [24] J. Y. Lee and S. M. Lee, *Surf. Coat. Technol.* **28**, 301 (1986).
- [25] M. Ichimura, Y. Sasajima, and M. Imabayashi, *Mater. Trans., JIM* **32**, 1109 (1991).
- [26] U. Stühr, T. Striffler, H. Wipf, H. Natter, B. Wettmann, S. Janssen, R. Hempelmann, and H. Hahn, *J. Alloys Compd.* **253–254**, 393 (1997).

- [27] T. Dieudonné, L. Marchetti, F. Jomard, M. Wery, J. Chêne, C. Allely, P. Cugy, and C. Scott, in *Defect and Diffusion Forum* (Trans Tech Publications, Switzerland, 2012), p. 477.
- [28] A. M. Brass and A. Chanfreau, *Acta Mater.* **44**, 3823 (1996).
- [29] R. M. Latanision and M. Kurkela, *Corrosion* **39**, 174 (1983).
- [30] J. Yao and J. R. Cahoon, *Acta Metall. Mater.* **39**, 119 (1991).
- [31] J. Yao and J. R. Cahoon, *Acta Metall. Mater.* **39**, 111 (1991).
- [32] A. Pedersen and H. Jónsson, *Acta Mater.* **57**, 4036 (2009).
- [33] A. Oudriss, J. Creus, J. Bouhattate, E. Conforto, C. Berziou, C. Savall, and X. Feugas, *Acta Mater.* **60**, 6814 (2012).
- [34] A. Oudriss, J. Creus, J. Bouhattate, C. Savall, B. Peraudeau, and X. Feugas, *Scr. Mater.* **66**, 37 (2012).
- [35] A. Oudriss, S. Le Guernic, Z. Wang, B. Osman Hoch, J. Bouhattate, E. Conforto, Z. Zhu, D. S. Li, and X. Feugas, *Mater. Lett.* **165**, 217 (2016).
- [36] X. Zhou, D. Marchand, D. L. McDowell, T. Zhu, and J. Song, *Phys. Rev. Lett.* **116**, 075502 (2016).
- [37] See Supplemental Material at <http://link.aps.org/supplemental/10.1103/PhysRevLett.122.215501> for more details on computational methods, equation derivation, and hydrogen diffusion analysis, which includes Refs. [38–51].
- [38] G. Kresse and J. Furthmüller, *Phys. Rev. B* **54**, 11169 (1996).
- [39] G. Kresse and J. Hafner, *Phys. Rev. B* **47**, 558 (1993).
- [40] G. Kresse and D. Joubert, *Phys. Rev. B* **59**, 1758 (1999).
- [41] J. P. Perdew, K. Burke, and M. Ernzerhof, *Phys. Rev. Lett.* **77**, 3865 (1996).
- [42] M. Methfessel and A. Paxton, *Phys. Rev. B* **40**, 3616 (1989).
- [43] G. Henkelman, B. P. Uberuaga, and H. Jónsson, *J. Chem. Phys.* **113**, 9901 (2000).
- [44] K. A. Fichthorn and W. H. Weinberg, *J. Chem. Phys.* **95**, 1090 (1991).
- [45] K. Binder, D. M. Ceperley, J.-P. Hansen, M. Kalos, D. Landau, D. Levesque, H. Mueller-Krumbhaar, D. Stauffer, and J.-J. Weis, *Monte Carlo Methods in Statistical Physics* (Springer Science + Business Media, Berlin, 2012), Vol. 7.
- [46] Y. Wang, D. Connétable, and D. Tanguy, *Acta Mater.* **103**, 334 (2016).
- [47] E. Wimmer, W. Wolf, J. Sticht, P. Saxe, C. B. Geller, R. Najafabadi, and G. A. Young, *Phys. Rev. B* **77**, 134305 (2008).
- [48] W. G. Perkins and D. R. Begeal, *Berichte Bunsenges. Phys. Chem.* **76**, 863 (1972).
- [49] J. P. Hirth, *Metall. Trans. A* **11**, 861 (1980).
- [50] A. Stukowski and K. Albe, *Model. Simul. Mater. Sci. Eng.* **18**, 085001 (2010).
- [51] A. Stukowski, V. V. Bulatov, and A. Arsenlis, *Model. Simul. Mater. Sci. Eng.* **20**, 085007 (2012).
- [52] M. Girod and B. Grammaticos, *Nucl. Phys. A* **330**, 40 (1979).
- [53] D. Di Stefano, M. Mrovec, and C. Elsässer, *Acta Mater.* **98**, 306 (2015).
- [54] Y. Fukai, *J. Alloys Compd.* **356–357**, 263 (2003).
- [55] D. Di Stefano, M. Mrovec, and C. Elsässer, *Phys. Rev. B* **92**, 224301 (2015).
- [56] Z. Hua, D. Wang, Z. Liu, Y. Zhang, and S. Zhu, *Mater. Lett.* **234**, 175 (2019).
- [57] O. A. Restrepo, N. Mousseau, M. Trochet, F. El-Mellouhi, O. Bouhali, and C. S. Becquart, *Phys. Rev. B* **97**, 054309 (2018).
- [58] Y. A. Du, J. Rogal, and R. Drautz, *Phys. Rev. B* **86**, 174110 (2012).
- [59] R. Kirchheim, *Prog. Mater. Sci.* **32**, 261 (1988).
- [60] T. Mütschele and R. Kirchheim, *Scr. Metall.* **21**, 135 (1987).
- [61] R. Bullough and B. Bilby, *Proc. Phys. Soc. London Sect. B* **69**, 1276 (1956).
- [62] B. A. Bilby, R. Bullough, and E. Smith, *Proc R. Soc. A* **231**, 263 (1955).
- [63] F. Frank, *Acta Metall.* **1**, 15 (1953).
- [64] A. McNabb and P. Foster, *Trans. Metall. Soc. AIME* **227**, 618 (1963).
- [65] H. Iwaoka, M. Arita, and Z. Horita, *Acta Mater.* **107**, 168 (2016).
- [66] M. Koyama, D. Yamasaki, T. Nagashima, C. C. Tasan, and K. Tsuzaki, *Scr. Mater.* **129**, 48 (2017).
- [67] M. Leonhardt, J. Jamnik, and J. Maier, *Electrochem. Solid-State Lett.* **2**, 333 (1999).
- [68] S. Couling and R. Smoluchowski, *J. Appl. Phys.* **25**, 1538 (1954).